# TURBULENCE MODEL ASSESSMENT FOR STALL DELAY APPLICATIONS AT LOW REYNOLDS NUMBER

**M. Arif Mohamed**

School of Mechanical and Aerospace Eng.
Nanyang Technological University
50 Nanyang Avenue, 639798, Singapore
mohd.arif@ntu.edu.sg email

**Martin Skote**

School of Mechanical and Aerospace Eng.
Nanyang Technological University
50 Nanyang Avenue, 639798, Singapore
mskote@ntu.edu.sg

**Yanhua Wu**

School of Mechanical and Aerospace Eng.
Nanyang Technological University
50 Nanyang Avenue, 639798, Singapore
yanhuawu@ntu.edu.sg

## ABSTRACT

This paper briefly looks at the results of three RANS (Reynolds-averaged Navier-Stokes) turbulence models that were used to simulate the stall delay phenomenon on a rotating wind turbine blade. It was found that all three models, namely the SST $k-\omega$, RNG $k-\varepsilon$ and realizable $k-\varepsilon$, where $k$, $\varepsilon$ and $\omega$ are turbulent kinetic energy, dissipation and specific dissipation rate respectively, produced non-physical normal stresses. All three models were still able to predict the stall delay phenomenon despite different distributions of velocity.

## INTRODUCTION

The fluid physics involved in three-dimensional wind turbine aerodynamics are complex. The reference to three-dimensionality in this context serves to point out the difference between flow over an aerofoil, which is a two-dimensional body, vis-à-vis a rotating wind turbine blade. Most notably, the advent of stall which is observed at a certain angle of attack (AOA) for an aerofoil is delayed for a wind turbine blade at the same AOA. The mechanism of this stall-delay phenomenon is still debatable. What is intriguing is the fact that despite many experimental studies performed on such flows, stall delay remains a 70-year-old mystery hitherto. While experiments in general provide pertinent flow information, there are many terms that are not measurable. Computational fluid dynamics (CFD) offers a route to these 'immeasurable terms'. However, CFD of such flows is not straight-forward. While the computations of direct numerical simulations (DNS) are highly sought after, they are not realistically feasible due to the high computational overheads. Large eddy simulations (LES), where the large scales are resolved and the small scales modelled, are a more realistic option where the dynamic Smagorinsky model (Germano *et al.*, 1991) in particular is purported to perform well for rotating flows (Squires & Piomelli, 1995). Reynolds-averaged Navier-Stokes (RANS) models offer a palliative in terms of computational costs but at the expense of less accurate predictions. Nevertheless these models are popular in wind engineering and are continuously being used. Here we discuss the issues with RANS models for stall-delay applications.

The choice of a RANS turbulence model is well-known to influence the results of such computations and therefore must be scrutinized with more depth than many studies such as Sagol *et al.* (2012) report. In other words, it is not only important to look at the aerodynamic loads on the blade such as the coefficients of pressure ($C_p$) but also the flow field scalars such as velocity magnitude and spanwise velocity. McCroskey & Yaggy (1968) argued that the latter contributes significantly to the delay of separation on rotating blades. In addition, at low Reynolds number (Re) local turbulence is said to have an unfavourable effect on the maximum lift on airfoils while the opposite is true for high Re (Stack, 1931). These important characteristics of the flow field suggest that several turbulence models must be considered for such applications because these standard models all come with their own deficiencies, corollary affecting the flow field. For example, the standard $k-\varepsilon$ turbulence model, where $k$ is turbulence and $\varepsilon$ is its dissipation rate, is known to suffer from the stagnation-point anomaly which sees an exaggeration of $k$ being produced in stagnation regions (see Durbin & Reif (2011)). This has important implications because $k$ is normally coupled with the pressure term in the RANS equations which means poor predictions of $k$ would result in pressure being poorly predicted as well (Castro, 1979). There have been improvements of the model in the form of the realizable $k-\varepsilon$ of Shih *et al.* (1995) and the RNG $k-\varepsilon$ of Yakhot *et al.* (1992) with the latter purported to perform better in rotating flows due to the incorporation of a swirl factor in the formulation of the eddy viscosity. Another model which is often being used in rotating flows is the SST $k-\omega$ of Menter (1994), where $\omega$ is specific dissipation rate. Yu *et al.* (2011) used the SST for the study of stall delay on the Phase VI rotor from the National Renewable Energy Laboratory (NREL) which is a two-bladed rotor of diameter 10.058 m with wind speeds ranging from 5 m/s to 10m/s at an angular velocity of 72 rpm. The results are generally in good agreement with experimental data barring some cases where there is massive flow separation. Note that the blade was designed using the S809 airfoil which Sørensen *et al.* (2002) claimed was suited for the computations with RANS particularly because the airfoil type is not sensitive to vortex interaction in the wake. Herráez *et al.* (2014) also used the SST model for a study into the rotational effects on the MEXICO wind turbine blade. They concluded that their simulations showed that drag reduces with rotation (unlike most other correction models for the effects of rotation), and that the current CFD models need more research when rotation is involved.

The aforementioned studies analyzed cases where Reynolds number is moderately high ($\geq 100,000$). This paper however looks to investigate the performance of simple turbulence models for rotor aerodynamics at low Re with emphasis on the stall delay phenomenon. This in itself presents a challenge not only because ro-

tation is involved but also because at low Re, simple two-equation turbulence models' prediction of the laminar or not-fully turbulent lengths can significantly affect the global flow field about the size of the object's geometric length as demonstrated by Rumsey & Spalart (2009). The realizable and RNG $k-\varepsilon$ as well as the SST $k-\omega$ are used in the current study to simulate the wind tunnel experiments of Lee & Wu (2015). The experiments focused on the stall delay phenomenon on a rotating/oscillating blade which was designed based on the S805 airfoil. In the experiments Re was 4300 and 4800 (based on the mid-chord and relative velocity), which are very low values but it is a good starting case for the evaluation of the models. Their experiments also focused on the effects of different turbulent intensities. However, in the present study, we will only be using one of them *viz.* 0.4 %. The tip-speed ratio (TSR) defined as $R\Omega/U_\infty$ where $R$, $\Omega$ and $U_\infty$ are blade radius, angular velocity and freestream velocity respectively, used for the current study is 3. The following section describes the methodology involved in setting up the case, while the next section discusses the results of the computations. A summary of the primary findings is presented in the last section.

## METHODOLOGY

The commercial code ANSYS Fluent 14.0 was used for the computations. The code uses the finite volume method to solve the RANS equations. The experiments of Lee & Wu (2015) were based on an blade that is oscillating. They mentioned that the flow field around a rotating blade (full rotation) can be replicated via oscillating motions. Based on this, the simulations were set to a steady state full rotation of the blade. The blade was rotated in an anti-clockwise direction when viewed from an upstream position so as to give it a lift component.

The computational mesh was generated in ANSYS ICEM. A quad mesh was mapped on the pressure and suction side of the blade while the cross sectional airfoil faces at the root and tip adopted a triangular patch. Ten prismatic layers were grown normal to the walls with a growth ratio of 1.03 and the first-node distance from the wall was refined until $y^+$ is unity. The inlet is placed 0.75 m upstream of the blade while the outlet is located 2.5 m downstream (See Figure 1). The inlet velocity was set to 1.62 m/s. As with the experiments of Lee & Wu (2015), a TSR of 3 mandates the rotating frame of reference having an angular velocity of 15.708 rad/s. Turbulence intensity was set to 0.4 % at the inlet. A series of grid tests were conducted to make sure the mesh was grid-independent. The chosen mesh consisted of 10, 550, 003 nodes.

## RESULTS AND DISCUSSION

We begin this section by showing the quantitative results of the experiments of Lee & Wu (2015) and the RANS simulations with different turbulence models. The TSR for this case equals 3 and Reynolds number is 4800. For a rotating blade, the coefficient of pressure $C_p$ is defined as

$$C_p = \frac{P_{\text{static}} - P_\infty}{0.5\rho(U^2_{\text{rotor}} + r^2\Omega^2)} \tag{1}$$

where $P_\infty$ and $P_{\text{static}}$ are ambient pressure (taken far upstream on the rotating blade) and static pressure respectively. $U_{\text{rotor}}$, $r$ and $\Omega$ represent the velocity at the rotor plane, local blade radius and angular velocity. The $C_p$ distribution on the suction side of the blade at different blade instances are depicted in Figure 2. As shown in Figure 2a , all three turbulence models were able to predict stall-delay albeit not matching the exact values of the experiments. At 0.25R, the SST predicted two peaks which suggests the possibility of a separation bubble in the region $0.05 \leq x/c \leq 0.16$. The profiles

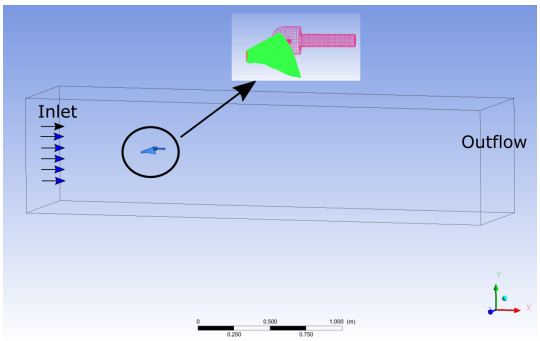


(a) Computational domain of the calculations. The top, bottom and the sides of the computational domain were set as inlet.

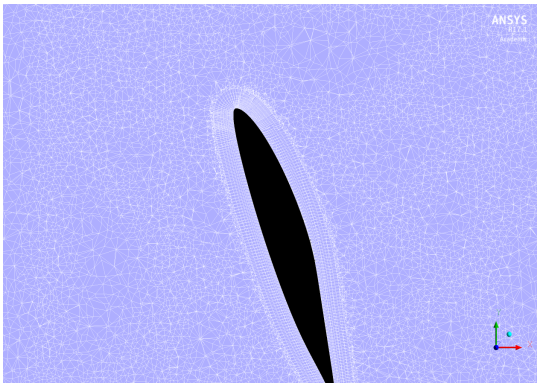

(b) A cut plane of the mesh depicting ten prismatic layers grown normal to the blade wall.

Figure 1: Computational domain and mesh of the model.

for $C_p$ for the three turbulence models remain almost unchanged at 0.55R and 0.75R. The realizable and RNG $k-\varepsilon$ continued to show a high lift component near the leading edge while the SST displayed a notably low peak very close to the leading edge at 0.55R and 0.75R. Interestingly enough, the RNG showed a good match of $C_p$ with the experiments at 0.55R.

The Reynolds stresses, $u_iu_j$ in two-equation models are not computed explicitly as they are in second moment closure models and as such they are modelled. The formulation for Reynolds stress in two-equation models is $u_iu_j = -2\nu_t S_{ij} + \frac{2}{3}k\delta_{ij}$ where $S_{ij}$ is the strain rate tensor.

One of the issues with this formulation is the possibility of negative normal stresses which is permissible if the first term on the left hand side eclipses the second term. Negative normal stresses are non-physical and violates the Cauchy-Schwartz inequality. A good way to show realistic, hence realizable, normal stresses is look at the phase-space portrait or the Lumley triangle. All non-realizable normal stresses occupy the space outside of the triangle. A virtual spherical volume was wrapped around the blade and hub and Reynolds stresses were extracted in this volume. Figure 3 shows the behaviour of the normal stresses via the Lumley triangle that are computed by the $k-\omega$, RNG $k-\varepsilon$ SST $k-\omega$ and realizable $k-\varepsilon$ turbulence models for the rotating case. It is immediately obvious that there is a substantial degree of non-realizable stresses computed by all models, surprisingly even in the realizable $k-\varepsilon$.

The contours of relative velocity magnitude normalized by the relative velocity $V_r$, defined as the modulus of the term in parenthesis of Equation (1), for all three models taken at the 0.25R plane are shown in Figure 4. As the emphasis of this study is on stall delay which occurs at the inboard, only the contours at 0.25R are shown. As seen, there is no indication of separation near the leading

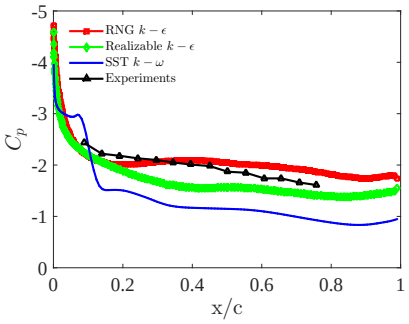


(a) 0.25R

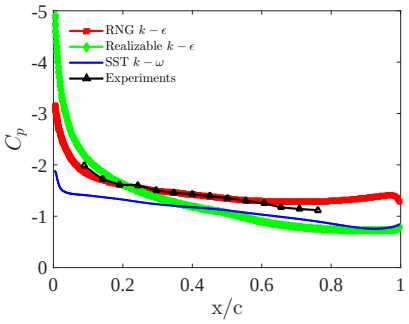


(b) 0.55R

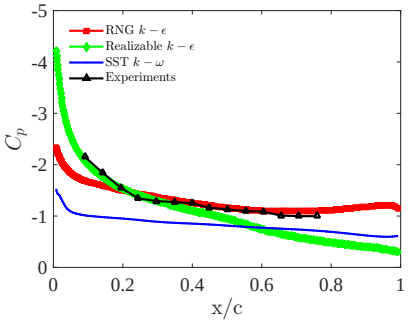


(c) 0.75R.

Figure 2: Distribution of $C_p$ along the suction side of the rotating blade predicted by the three turbulence models. TSR was set at 3 for Reynolds number 4800.

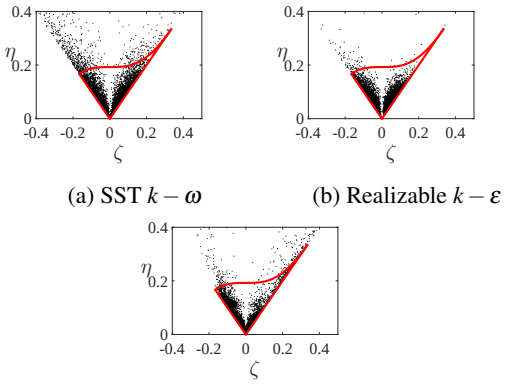


(a) SST $k-\omega$ (b) Realizable $k-\epsilon$

(c) RNG $k-\epsilon$

Figure 3: Space portrait of the Reynolds stresses.

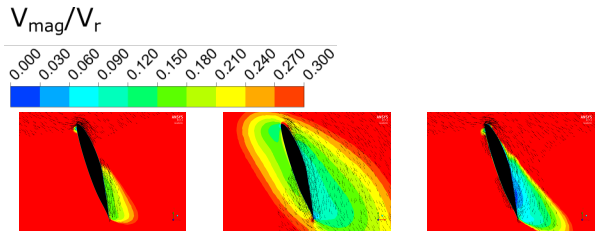


(a) Realizable $k-\varepsilon$ (b) RNG $k-\varepsilon$ (c) SST $k-\omega$

Figure 4: Distribution of normalized velocity magnitude $V_{mag}$ at 0.25R with TSR = 3.

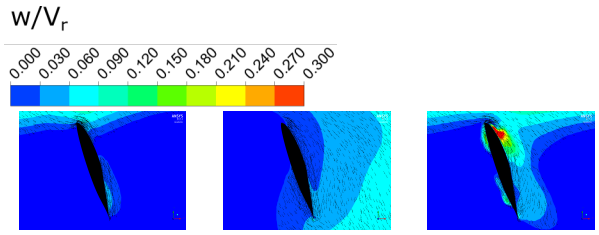


(a) Realizable $k-\varepsilon$ (b) RNG $k-\varepsilon$ (c) SST $k-\omega$

Figure 5: Distribution of normalized spanwise velocity $w$ at 0.25R with TSR = 3.

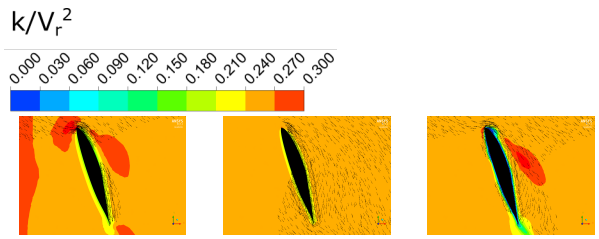


(a) Realizable $k-\varepsilon$ (b) RNG $k-\varepsilon$ (c) SST $k-\omega$

Figure 6: Distribution of normalized $k$ at 0.25R with TSR = 3.

edge for all three models (separation is indicated by the dark blue regions) although the SST predicted a small re-circulation region near the leading edge explaining the two peaks in Figure 2a. It is interesting to note that the $V_{mag}/V_r$ distribution from the RNG $k-\varepsilon$ calculations is closest to resemble the experimental results. The realizable $k-\varepsilon$ predicted higher concentration of $V_{mag}/V_r$ around the airfoil as compared to the other two cases.

As mentioned earlier, spanwise velocity $w$ can help delay separation and as shown in Figure 5, all three models showed positive $w/V_r$. Positive $w$ indicate radial flow towards the tip of the blade. The RNG predicted the least concentration near the leading edge. This is not surprising considering it predicted the lowest $V_{mag}$ amongst the three models. The SST showed the highest $w$ near the leading edge on the suction side. The normalized $k$ distribution is shown in Figure 6. The SST predicted the least turbulence near the leading edge. Interestingly enough, this distribution of low $k$ relative to the predictions of the other two models seem to produce a lower $C_p$. This is contrary to an airfoil as mentioned in the Introduction. Furthermore, these low values of $k$ near the wall could be

due to the fact that the SST does not incorporate a wall function unlike the other two models, and also because of the cross diffusion term in the SST which dampens turbulence.

## CONCLUSIONS

Three turbulence models namely the RNG $k-\varepsilon$, Realizable $k-\varepsilon$ and the SST $k-\omega$ were used to simulate the stall-delay phenomenon on the S805 wind turbine blade. It should be promulgated that none of these models should be used when investigating Reynolds stresses due to non-realizable behavior shown by all models (even the realizable $k-\varepsilon$). The results also show vast different behaviors of velocity between the three models even though the all three models predicted the delay of stall via the surface pressure distributions on the blade.

## REFERENCES


Castro, IP 1979 Numerical difficulties in the calculation of complex turbulent flows. In *Turbulent Shear Flows I*, pp. 220–236. Springer.

Durbin, Paul A & Reif, BA Pettersson 2011 *Statistical theory and modeling for turbulent flows*. John Wiley & Sons.

Germano, Massimo, Piomelli, Ugo, Moin, Parviz & Cabot, William H 1991 A dynamic subgrid-scale eddy viscosity model. *Physics of Fluids A: Fluid Dynamics (1989-1993)* **3** (7), 1760–1765.

Herráez, Iván, Stoevesandt, Bernhard & Peinke, Joachim 2014 Insight into rotational effects on a wind turbine blade using navier–stokes computations. *Energies* **7** (10), 6798–6822.

Lee, Hsiao Mun & Wu, Yanhua 2015 A tomo-piv study of the effects of freestream turbulence on stall delay of the blade of a horizontal-axis wind turbine. *Wind Energy* **18** (7), 1185–1205.

McCroskey, WJ & Yaggy, PF 1968 Laminar boundary layers on helicopter rotors in forward flight. *AIAA journal* **6** (10), 1919–1926.

Menter, Florian R 1994 Two-equation eddy-viscosity turbulence models for engineering applications. *AIAA journal* **32** (8), 1598–1605.

Rumsey, Christopher L & Spalart, Philippe R 2009 Turbulence model behavior in low reynolds number regions of aerodynamic flowfields. *AIAA journal* **47** (4), 982–993.

Sagol, Ece, Reggio, Marcelo & Ilinca, Adrian 2012 Assessment of two-equation turbulence models and validation of the performance characteristics of an experimental wind turbine by cfd. *ISRN Mechanical Engineering* **2012**.

Shih, Tsan-Hsing, Liou, William W, Shabbir, Aamir, Yang, Zhigang & Zhu, Jiang 1995 A new $k$-$\varepsilon$ eddy viscosity model for high reynolds number turbulent flows. *Computers & Fluids* **24** (3), 227–238.

Sørensen, Niels N, Michelsen, JA & Schreck, S 2002 Navier–stokes predictions of the nrel phase vi rotor in the nasa ames 80 ft$\times$ 120 ft wind tunnel. *Wind Energy* **5** (2-3), 151–169.

Squires, Kyle D & Piomelli, Ugo 1995 Dynamic modeling of rotating turbulence. In *Turbulent Shear Flows 9*, pp. 71–83. Springer.

Stack, John 1931 Tests in the variable density wind tunnel to investigate the effects of scale and turbulence on airfoil characteristics .

Yakhot, VSASTBCG, Orszag, SA, Thangam, S, Gatski, TB & Speziale, CG 1992 Development of turbulence models for shear flows by a double expansion technique. *Physics of Fluids A: Fluid Dynamics (1989-1993)* **4** (7), 1510–1520.

Yu, Guohua, Shen, Xin, Zhu, Xiaocheng & Du, Zhaohui 2011 An insight into the separate flow and stall delay for hawt. *Renewable Energy* **36** (1), 69–76.